SIAM J. SCI. COMPUT.
Vol. 19, No. 4, pp. 1290–1302, July 1998
© 1998 Society for Industrial and Applied Mathematics
013

ON THE ACCURACY OF IMPULSE METHODS FOR FLUID FLOW*

RICARDO CORTEZ†

Abstract. A Lagrangian numerical method based on impulse variables is analyzed. The relation between discrete impulse vectors and vortex dipoles with a prescribed dipole moment is presented and used to adapt the high-accuracy cutoff functions of vortex methods for use in impulse-based methods. The long-time implementation of the impulse method is shown to contain a source of error whose growth in time leads to a severe loss of accuracy in interior flows. Applications for which impulse methods are well suited are identified.

Key words. impulse variables, vortex dipoles, vortex methods

AMS subject classifications. 65C20, 65G99, 76C99

PII. S1064827595293570

1. Introduction. The Navier–Stokes equations are typically written in terms of the fluid velocity or vorticity. Most numerical methods are discretizations of either formulation of these equations. The introduction of impulse variables [7] (which have been also called magnetization [8, 9, 13, 22], velicity [8], and impetus [23]) has led to a new formulation of the fluid equations [25, 8, 30]. In terms of the new variables, the Euler equations display readily the Hamiltonian structure of fluid flow in any space dimension. Buttke [8] introduced a Lagrangian numerical method for Euler flow based on discretizations of the impulse equations. These discretizations lead to systems which conserve many invariants associated with the Hamiltonian. However, many questions regarding the method remained unresolved. For instance, specific flows for which the method is particularly useful have not been identified, the accuracy of impulse-based methods has not been studied for long-time implementations, and convergence properties of the method and how to choose the cutoff functions were unknown. These questions are answered here. We present an argument that shows that the impulse blob discretizations used in [8] induce the same flow as smoothed vortex dipoles. Consequently, the particle locations obtained with the impulse method approximate the locations obtained with a vortex method which uses the same smoothing parameters. This result allows one to import the role of the cutoff function used in vortex methods into impulse methods and validates the use of such functions in the present context.

We also show that the impulse flow is an approximation to the flow induced by appropriately smoothed vortex sheets and that this approximation depends on the particle distribution along the sheet. In the impulse method as presented in [8], this approximation loses accuracy as the vortex sheets stretch. The stretching of the vortex sheets is directly related to the growth of the magnitude of the impulse vectors defined on the sheet. A consequence of this result is that accurate long-time implementations of the method in interior flows require modifications of the method. In section 4 we present numerical examples that illustrate the results, including a variation of the

* Received by the editors October 18, 1995; accepted for publication (in revised form) October 4, 1996; published electronically April 16, 1998.
http://www.siam.org/journals/sisc/19-4/29357.html
† Courant Institute of Mathematical Sciences, 251 Mercer Street, New York, NY 10012 (cortezr@cims.nyu.edu). This work was supported in part by the Applied Mathematical Sciences Subprogram of the Office of Energy Research, U.S. Department of Energy under contract DE-AC03-76SF00098 and by the Air Force Office of Scientific Research AASERT Grant FDF49620-93-1-0053.

impulse method which maintains the initial accuracy. However, the practicality of this and other possible modifications is questionable.

There are applications for which impulse methods are very useful. For example, problems of immersed boundaries with surface forces can be modeled with impulse variables since these represent dipoles and the impulse equations update the dipole strengths appropriately. One instance of such an application is found in [16], where the motion of a thin elastic membrane surrounding a fluid was modeled. Other applications of impulse methods include flow near solid boundaries. Summers and Chorin [34] have used a combination of impulse and vortex elements to model viscous flow past a sphere.

This paper begins with the equations of motion for impulse and a brief presentation of the velocity field given by the impulse method. In section 3 we show the connection between impulse and vortex dipoles and the relevance of this connection on the accuracy of the impulse method in long-time implementations. Numerical examples that illustrate the results are presented in section 4. A discussion of applications of impulse methods which do not present accuracy problems and for which impulse methods seem particularly attractive is presented in the concluding section.

2. Equations of motion. Let $\mathbf{u}$ be the velocity of an incompressible fluid. Impulse can be introduced starting with the fluid velocity at time $t = 0$ and making a change of variables in the following way: let $\mathbf{m}$ be a vector field equivalent to $\mathbf{u}$ up to an arbitrary gradient; that is,

$$\mathbf{m} = \mathbf{u} + \nabla\phi. \tag{2.1}$$

Since $\nabla \cdot \mathbf{u} = 0$, equation (2.1) implies that $\mathbf{u}$ is the divergence-free part of the Hodge decomposition of $\mathbf{m}$ in free space (see [14]). This fact will be written symbolically as $\mathbf{u} = \mathbb{P}\mathbf{m}$. In two dimensions it is known that ϕ can be chosen in such a way that $\mathbf{m}$ has compact support only when the net vorticity is zero. The equations of motion for $\mathbf{m}$ in free space of any dimension are (see, e.g., [8, 9, 16])

$$\frac{D\mathbf{m}}{Dt} = -(\nabla\mathbf{u})^T\mathbf{m} + \nu\Delta\mathbf{m}, \qquad \mathbb{P}\mathbf{m} = \mathbf{u}, \tag{2.2}$$

where $D/Dt = \partial/\partial t + \mathbf{u}\cdot\nabla$ is the derivative along particle trajectories, $\nabla\mathbf{u}$ is a matrix with entries $(\nabla\mathbf{u})_{ij} = \partial u_i/\partial x_j$, and T denotes a transpose. For a derivation of (2.2) refer to [8, 16]. By substituting (2.1) into (2.2) we can check that the latter is consistent with the Navier–Stokes equations. In the remainder of this paper we consider Euler flow, so we set $\nu = 0$ and reduce the impulse equations to

$$\frac{D\mathbf{m}}{Dt} = -(\nabla\mathbf{u})^T\mathbf{m}, \qquad \mathbb{P}\mathbf{m} = \mathbf{u}. \tag{2.3}$$

One can define families of functions, parametrized by time, so that the gradients of those functions evolve with the same equation as $\mathbf{m}$. We will make use of such functions, and so we state a result which is found and proved in [15]. Let ϕ_t denote the flow map so that $\phi_t(\alpha) = \mathbf{x}(\alpha, t)$, where $\mathbf{x}(\alpha, t)$ is the trajectory followed by the particle which is initially at position α. For the following proposition we assume that all functions, including the fluid velocity and the flow map, are smooth.

PROPOSITION 2.1. *Let $P_0 : \mathbb{R}^n \to \mathbb{R}$ ($n = 2$ or 3) be smooth and let $P_0(\alpha) = 0$ implicitly define a surface S_0. Define the family of functions $P_t(\mathbf{x}) = P_0 \circ \phi_t^{-1}(\mathbf{x})$ parametrized by time and assume that there is some function H_0 defined on S_0 such*

that $\mathbf{m}$ *is initially given by* $\mathbf{m}(\alpha,0) = H_0(\alpha)\nabla P_0(\alpha)$. *Then the equations of motion for* ∇P_t *and* $\mathbf{m}$ *are identical and*

$$\mathbf{m}(\mathbf{x},t) = H_0(\alpha)\ \nabla P_t(\mathbf{x}),$$
$$\xi(\mathbf{x},t) = \nabla H_t(\mathbf{x}) \times \nabla P_t(\mathbf{x}),$$

where $H_t(\mathbf{x}) = H_0 \circ \phi_t^{-1}(\mathbf{x})$, $P_t(\mathbf{x}) = P_0 \circ \phi_t^{-1}(\mathbf{x})$, *and* $\alpha = \phi_t^{-1}(\mathbf{x})$.

This result holds true for any smooth velocity field $\mathbf{u}$, as long as $\mathbf{m}$ evolves according to (2.3). Proposition 2.1 states that if $\mathbf{m}$ is initially proportional to the gradient of some function P_0 on the surface S_0, then $\mathbf{m}$ will remain proportional to ∇P_t on the image of S_0 under the flow map. Consequently, $\mathbf{m}$ will evolve in such a way that it remains perpendicular to the surface $S_t = S(\phi_t(S_0)) = \{\mathbf{x} \in \mathbb{R}^2 : P_t(\mathbf{x}) = 0\}$. In [15], these surfaces which remain perpendicular to $\mathbf{m}$ during the evolution of the flow are referred to as $\mathbf{m}$-*orthogonal surfaces*.

During the evolution of the flow, the area of an $\mathbf{m}$-orthogonal surface may change even when the flow is incompressible since the flow can accommodate larger areas by contracting in the direction normal to the surface. The growth of the area of an $\mathbf{m}$-orthogonal surface is proportional to the local growth of the magnitude of $\mathbf{m}$. This result has been discussed in [9] and [12] by interpreting the flow induced by an impulse vector as that of a small vortex loop. This issue is key in the numerical method, where discrete impulse vectors carry elements of volume. Each volume element can be thought of as the area of a piece of an $\mathbf{m}$-orthogonal surface multiplied by a thickness, where the length of each vector is proportional to the area it carries. In section 3 we will show that the accuracy of the method depends on the distribution of particles on the $\mathbf{m}$-orthogonal surfaces, and those surfaces in the interior of a flow can develop regions where particles are sparse, leading to a catastrophic loss of accuracy.

3. The Lagrangian numerical method. The equations of motion along fluid particles are

$$\frac{d}{dt}\mathbf{x}(\alpha,t) = \mathbf{u}(\mathbf{x}), \qquad \mathbf{x}(\alpha,0) = \alpha, \tag{3.1}$$

$$\frac{d}{dt}\mathbf{m}(\mathbf{x},t) = -(\nabla\mathbf{u})^T\mathbf{m}(\mathbf{x},t), \qquad \mathbf{m}(\alpha,0) = \text{given}. \tag{3.2}$$

In [8], the impulse field is discretized initially by subdividing the domain into cells with the volume (or area) of the jth cell equal to V^j and by letting $\mathbf{m}^j = \mathbf{m}(\alpha^j)V^j$, where α^j is the center of the cell. Then an approximate impulse field is given by the sum

$$\tilde{\mathbf{m}}(\mathbf{x}) = \sum_{j=1}^{N} \mathbf{m}^j(t) f_\delta(\mathbf{x} - \mathbf{x}^j), \tag{3.3}$$

where N is the total number of cells and f_δ is a smooth approximation of a Dirac delta function. The smoothing functions used in [8] were taken from vortex methods; however, no discussion about this choice was presented. More recently there has been some evidence that indicates that cutoff functions from vortex methods are in fact the appropriate choice [16]. In the next section we show that the choice of cutoffs in (3.3) is associated with the same choice of cutoff functions in a vortex method.

If we assume that the cutoff function f_δ is radially symmetric, we find that in two

dimensions the velocity at $\mathbf{x}$ is given by

$$\mathbf{u}(\mathbf{x}) = \frac{1}{2\pi}\sum_{j=1}^{N} \mathbf{m}^j \left[\frac{rF'(r) - F(r)}{r^2}\right] - \hat{\mathbf{r}}^j(\mathbf{m}^j \cdot \hat{\mathbf{r}}^j)\left[\frac{rF'(r) - 2F(r)}{r^2}\right], \tag{3.4}$$

where $\hat{\mathbf{r}}^j = (\mathbf{x} - \mathbf{x}^j)/r$ and $r = |\mathbf{x} - \mathbf{x}^j|$. The function $F(r) = \int_{|\mathbf{x}|\le r} f_\delta(|\mathbf{x}|)d\mathbf{x}$ is the shape factor and depends only on the choice of cutoff functions. The impulse vectors $\mathbf{m}^j$ evolve with an equation that approximates (3.2) and is found by direct differentiation of the velocity expression above [8, 9, 16].

3.1. Discrete impulse and vortex blobs in $\mathbb{R}^2$. Suppose there is a single impulse blob located at the origin. The velocity at an arbitrary point $\mathbf{x}$ due to the impulse can be written as [15]

$$\mathbf{u}(\mathbf{x}) = \nabla \times (K * f_\delta)\mathbf{m} = K * (\nabla \times \mathbf{m} f_\delta), \tag{3.5}$$

where $K(x, y) = (-y, x)/2\pi(x^2 + y^2)$ is the vortex kernel. Equation (3.5) is the velocity field due to the vorticity $\xi(\mathbf{x}) = \nabla \times \mathbf{m} f_\delta(\mathbf{x})$ induced by the smooth impulse vector. If we write $\xi = (0, 0, \omega)^T$ we have that

$$\omega(\mathbf{x}) = \nabla f_\delta(\mathbf{x}) \cdot (\mathbf{m} \times \hat{\mathbf{z}}),$$

where $\hat{\mathbf{z}}$ is the unit vector normal to the plane. Thus, one can interpret the vorticity as $|\mathbf{m}|$ times the derivative of the cutoff function f_δ in the direction of $(\mathbf{m} \times \hat{\mathbf{z}})$. Let $\mathbf{h}$ represent a vector in the direction of $(\mathbf{m} \times \hat{\mathbf{z}})$ and let $|\mathbf{h}| = h$. Then, the vorticity may be written as

$$\omega(\mathbf{x}) = \lim_{h\to 0} \omega\big[f_\delta(\mathbf{x} + \mathbf{h}) - f_\delta(\mathbf{x} - \mathbf{h})\big], \tag{3.6}$$

where $\omega = |\mathbf{m}|/2h$. This expression shows explicitly that the vorticity induced by the discrete impulse is that of vortex dipoles (see Figure 3.1). A vortex dipole is the limit of two vortex blobs of equal and opposite strength as their separation goes to zero; this limit is taken in a way that maintains a constant dipole moment equal to $-2\mathbf{h}\omega = (\hat{\mathbf{z}} \times \mathbf{m})$ (see, e.g., [5]).

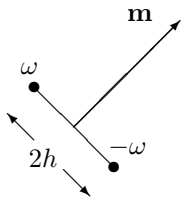

FIG. 3.1. *Vortex pair approximation to impulse vector.*

An important conclusion is that the impulse discretization in (3.3) is equivalent to a distribution of dipoles along $\mathbf{m}$-orthogonal surfaces. Therefore, the $\mathbf{m}$-orthogonal surfaces are vortex sheets, although these vortex sheets are slightly unconventional in the sense that the vorticity distribution along them may be discontinuous and may contain portions with zero vorticity.

To a given accuracy, the limit in (3.6) can be approximated by placing the two vortices a small distance apart. The resulting vorticity is that of a vortex blob discretization which uses the same cutoff function as the impulse discretization. The cutoff functions from vortex methods are therefore the appropriate blobs for the impulse method, and thus the relations between h and the cutoff radius δ required in vortex methods [1, 6, 17, 18, 28, 33] must be respected in the present context too. It is clear that for a small value of h and a given final time, the particle locations given by the impulse method must approximate well the particle locations obtained with a vortex method which uses the same cutoff function and radius. Our numerical experiments demonstrate this result.

We turn now to a discussion of the mechanism that causes the impulse method as presented in [8] to lose accuracy in time. We present the analysis in terms of the induced velocity field. If a vortex sheet has net vorticity zero, then the velocity at an arbitrary point due to this vorticity can be written as an line integral along the curve; the velocity due to impulse vectors which represent the same flow is a discretization of this integral.

3.2. The velocity field. Consider a finite vortex sheet with parametric representation $\mathbf{x}(s)$, where s is the arclength parameter with $s = 0$ at the left end of the curve and $s = 1$ at the right end. Assume that the net vorticity is zero and define $\Gamma(s) = \int_0^s \omega(\mathbf{x}(q))dq$. From this definition it is clear that $\Gamma(0) = 0$ and $\Gamma(1) = \int_0^1 \omega(\mathbf{x}(q))dq = 0$ by assumption. With the vortex method the velocity field is computed by using a smoothed vortex kernel of the type $K_\delta(x, y) = K(x, y)F(r)$, where $F(r)$ is the shape factor defined at the beginning of section 3. When the velocity field is approximated by $\mathbf{u}_\delta = K_\delta * \omega$, we have

$$\begin{aligned}\mathbf{u}_\delta(\mathbf{x}) &= \int_0^1 \omega(\mathbf{x}(s))\ K_\delta(\mathbf{x}-\mathbf{x}(s))ds = \int_0^1 \left[\frac{d}{ds}\Gamma(s)\right] K_\delta(\mathbf{x}-\mathbf{x}(s))ds \\ &= -\int_0^1 \Gamma(s)\ \left[\frac{d}{ds}K_\delta(\mathbf{x}-\mathbf{x}(s))\right] ds,\end{aligned}$$

where the last equation follows after integration by parts. Note that $\frac{d}{ds}K_\delta(\mathbf{x}-\mathbf{x}(s)) = -(\nabla K_\delta)\mathbf{x}'(s)$, where $\mathbf{x}'(s)$ is the unit vector tangent to the curve. Upon calculating (∇K_δ), we find that

$$2\pi\nabla K_\delta(\mathbf{x}-\mathbf{x}(s))\ \mathbf{x}'(s) = -\left[\hat{\mathbf{r}}(s)\cdot(\hat{\mathbf{z}}\times\mathbf{x}')\right]\hat{\mathbf{r}}(s)\left[\frac{rF'-2F}{r^2}\right] + (\hat{\mathbf{z}}\times\mathbf{x}'(s))\left[\frac{rF'-F}{r^2}\right],$$

where $r = |\mathbf{x}-\mathbf{x}(s)|$ and $\hat{\mathbf{r}}(s) = (\mathbf{x}-\mathbf{x}(s))/r$. Therefore,

$$\mathbf{u}_\delta(\mathbf{x}) = \frac{1}{2\pi}\int_0^1 \mathbf{m}(s)\left[\frac{rF'-F}{r^2}\right] - \Big(\hat{\mathbf{r}}(s)\cdot\mathbf{m}(s)\Big)\hat{\mathbf{r}}(s)\left[\frac{rF'-2F}{r^2}\right] ds, \tag{3.7}$$

where $\mathbf{m}(s) = \Gamma(s)\ (\hat{\mathbf{z}}\times\mathbf{x}'(s))$ is normal to the vortex sheet. Equation (3.7) gives the velocity induced by a smoothed vortex sheet and (3.4) is a discretization of this integral.

At $t = 0$ the impulse discretization can be arranged along the vortex sheet in such a way that (3.4) may represent a standard quadrature rule approximating the integral in (3.7). As the flow evolves the vortex sheet will stretch and wrap around itself [21, 32] creating regions where the particles carrying impulse are far apart from their neighbors. This mechanism causes the flow to be one induced by a collection

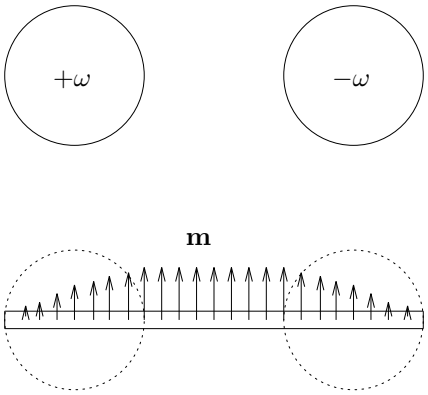

FIG. 3.2. *Two patches of constant vorticity (top). The bottom picture shows the corresponding impulse field defined on a horizontal sheet.*

of vortex dipoles sparsely placed along the sheet and not the flow induced by a good approximation of the vortex sheet.

In practice, one discretizes impulse by identifying many sheets in which the impulse vectors can be defined. For example consider the problem of two vortex patches of constant vorticity $+\omega$ and $-\omega$ as shown in Figure 3.2. Impulse vectors can be defined along horizontal sheets as shown in the figure where $\mathbf{m} = (0, m_2)$, with $m_2(x, y) = \int^x \omega(\zeta, y) d\zeta$.

4. Numerical examples. We present two numerical experiments designed to illustrate the loss of accuracy in the approximation of the velocity integral discussed above.

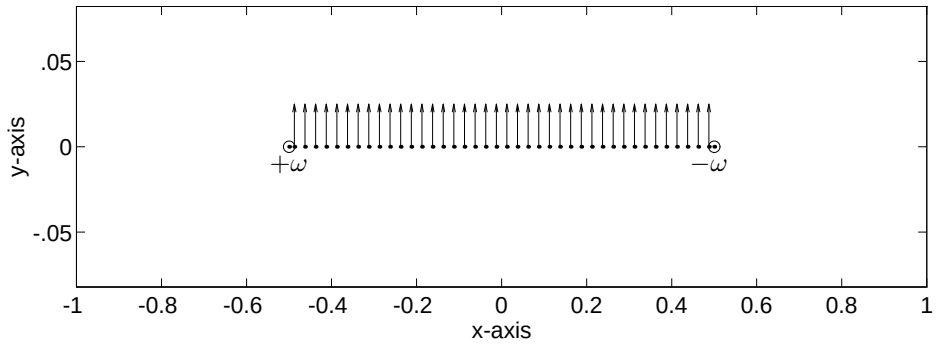

FIG. 4.1. *Initial impulse which represents the flow induced by two vortex blobs of equal and opposite strength.*

4.1. Numerical experiment I: Two vortex blobs. The first example consists of the flow induced by two point vortices of equal but opposite strength ω as shown in Figure 4.1. The positive and negative vortices are located initially at $(\pm 1/2, 0)$. The initial impulse is $\mathbf{m} = (0, \omega)^T$ on the line segment connecting the two vortices and zero elsewhere. The interval $[-1/2, 1/2]$ on the x-axis was divided into N intervals

of length $h = 1/N$, and the initial impulse vectors were placed at the center of each interval. With this setup, the velocity induced by the impulse represents the midpoint rule approximation of the velocity field obtained with a vortex method which uses the same cutoff function. The initial vortex sheet of this example is the segment $[-1/2, 1/2]$ with vortex blobs at the endpoints and zero vorticity elsewhere. This initial sheet is a natural choice for the support of impulse. However, any curve connecting the two endpoints can be chosen, and each choice would correspond to a different gauge in (2.1). As the flow evolves and the vortex sheet wraps around the vortices, the impulse vectors become sparsely distributed along the sheet, and one can expect the midpoint rule along such an integration path to experience accuracy loss. The solution was found first with the corresponding vortex method keeping track of the location of the vortices and of marker particles placed initially where the impulse vectors start out. The same problem was then solved using the impulse method (see Figure 4.2). Both methods used the cutoff radius $\delta = 0.3$ and the second-order cutoff function $f_\delta(r) = \delta^{-2} f_1(r/\delta)$, where $f_1(r) = \frac{1}{2\pi}(e^{-r^2} + \frac{1}{2}e^{-r^2/2})$.

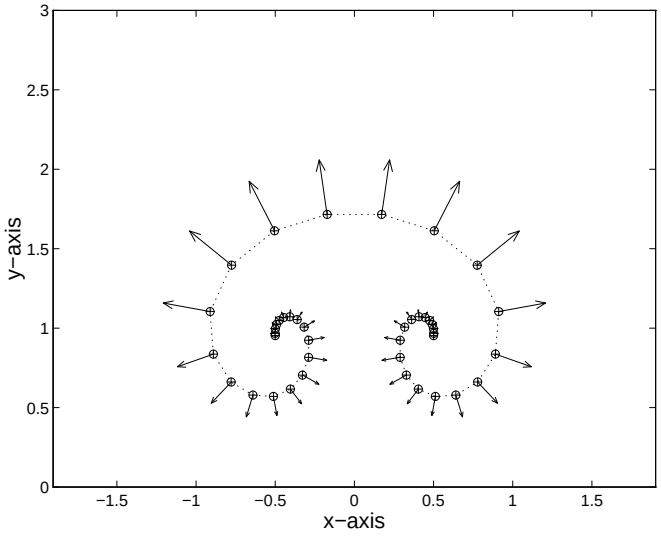

FIG. 4.2. *Solutions at time $t = 6$ obtained with a vortex method ($\oplus$) and the impulse method (arrows).*

Define the error

$$Error = \frac{1}{N}\sum_{j=1}^{N} |\mathbf{x}_V^j - \mathbf{x}_I^j|, \tag{4.1}$$

where $\mathbf{x}_V^j$ is the location of the jth particle obtained with the vortex method and $\mathbf{x}_I^j$ is the location obtained with the impulse method. Figure 4.3 shows the variation of this error in time for $\omega = 1$ and for two different discretizations corresponding to $N = 40$ and $N = 80$. For a given initial discretization, there is a critical time after which the error grows unboundedly. This problem is also encountered in computations using vortex methods in interior flows. However, the problem is more severe in impulse methods because the integrands being approximated involve derivatives of the vortex kernel (second derivatives in (3.2)), and these introduce larger quadrature errors. As

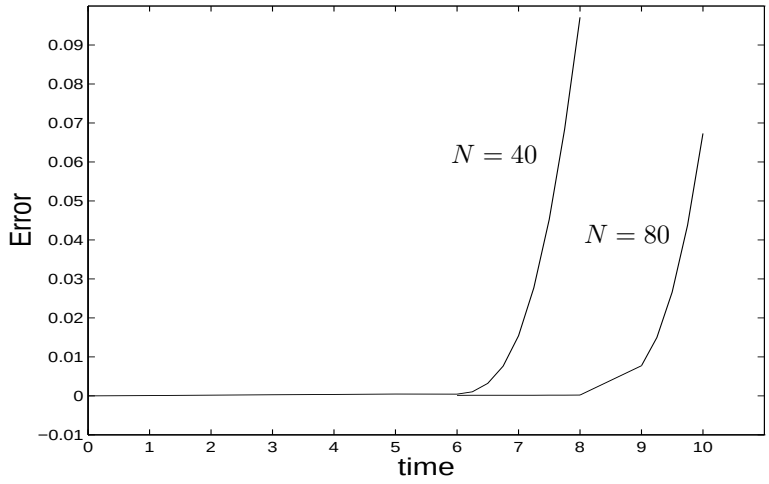

FIG. 4.3. *Error in particle positions for the impulse method for time* $0 \leq t < 10$ *and discretizations corresponding to* $N = 40$ *and* $N = 80$. *The error was defined as the average difference in particles' positions evolved once with the vortex method and once with the impulse method.*

expected, a finer discretization allows the impulse method to maintain good accuracy for longer times. In both cases, the sharp increase of the error occurred when the largest separation between contiguous vectors was of the order of the cutoff parameter δ. Different choices of initial gauge may delay the onset of error blow-up, but ultimately the results would be the same. It is clear that in long-time implementations, the impulse vectors eventually drift so far apart on the **m**-orthogonal surface that they do not approximate the vortex flow; the impulse flow is that of vortex dipoles at the base of the vectors. We point out that even as the impulse method loses the accuracy with which it approximates the flow induced by the two vortices, the invariants associated with the Hamiltonian dipole system continue to be preserved to an accuracy of 10^{-8}.

4.2. Numerical experiment II: Two vortex patches. The second experiment consists of two circular vortex patches of radius 0.25, strengths $+1$ and -1, and centered at $(-0.5, 0)$ and $(0.5, 0)$, respectively. The patches were discretized with vortex blobs, and this discretization was approximated by impulse vectors. In the impulse method, the vectors were placed along horizontal vortex sheets as in Figure 3.2. In this case, the parameters used were $\delta = 0.5$ and the initial interparticle spacing $h = 0.05$. The particles were evolved with the impulse method to time $t = 4.76$, and the positions of the vortices were compared with the ones obtained with the vortex method. Figure 4.4 shows the location of the vortices (circles) and impulse vectors (dots) given by the impulse method at $t = 4.76$ as well as the locations of the vortices obtained with the vortex method. The results clearly indicate that the position and shape of the patches given by the impulse method are incorrect.

The accuracy in the impulse approximation of the velocity field can be maintained by dynamically introducing new impulse vectors throughout the evolution of the flow, whenever the separation between contiguous vectors surpasses a predetermined tolerance. This refinement is done only in the approximation of the vortex flow by impulse vectors, not to new vortex blob discretizations of the patches. The number of vortex blobs is fixed at the beginning of the problem. In the refinement

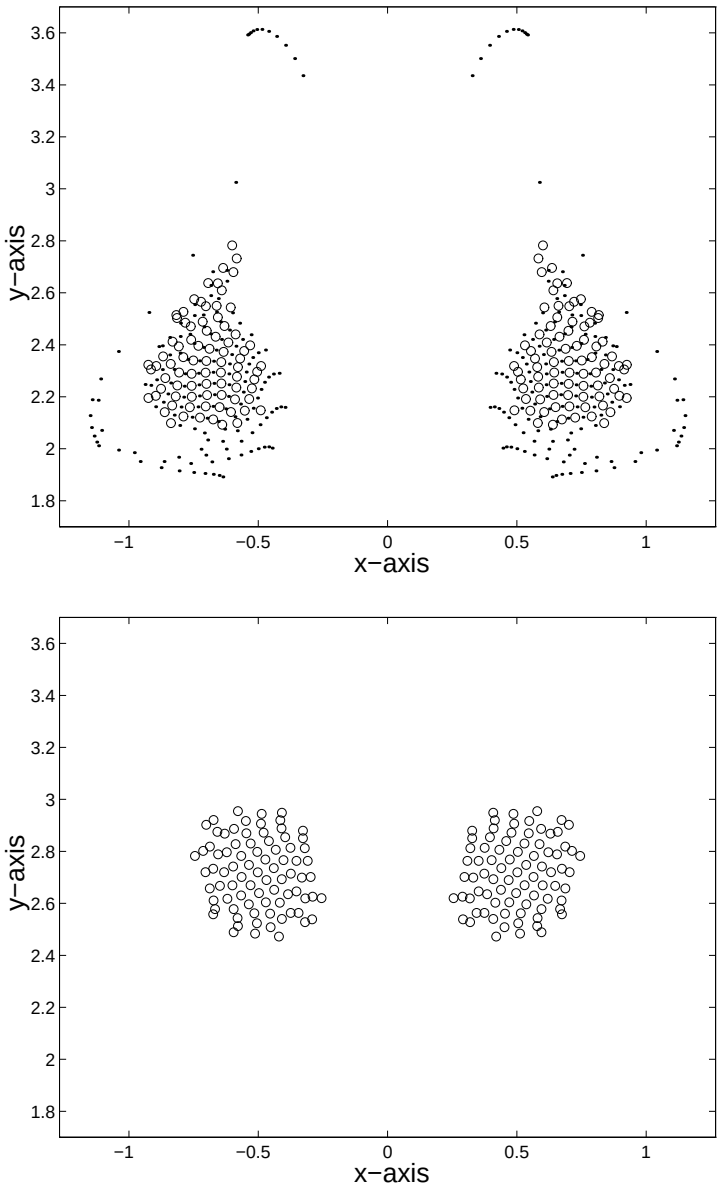

FIG. 4.4. *Solution at* $t = 4.76$. *The top figure shows the vortex locations (circles) and the location of the impulse vectors (dots) obtained with the impulse method. The bottom figure shows the location of the vortices obtained with the vortex method.*

procedure we consider the **m**-orthogonal surfaces as piecewise linear curves with a vector at the midpoint of each linear piece (see Figure 4.5). When the size of a linear piece exceeds the tolerance, we replace that vector by two equally spaced vectors in the same direction and with half the magnitude of the original one. This procedure is designed to preserve the discrete impulse, $\mathbf{I} = \sum \mathbf{m}^j$, exactly.

The results for time $t = 4.72$ are shown in Figure 4.6. In this case, an impulse vector was replaced by two vectors whenever the discretization size (the interparticle

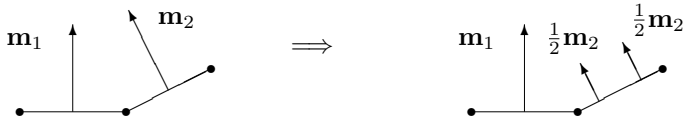

FIG. 4.5. *Refinement procedure which preserves impulse.*

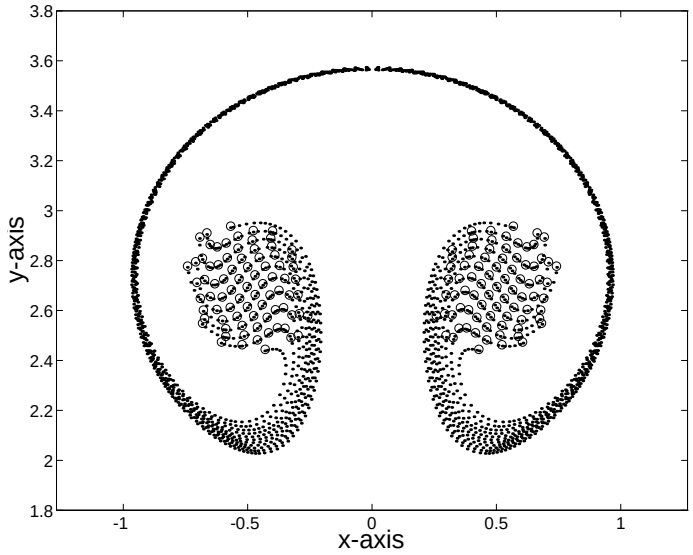

FIG. 4.6. *Solution at $t = 4.72$ found with the impulse method with refinement.*

spacing) reached twice the initial value. In comparison with Figure 4.4, it is clear that the refinement procedure allows the impulse method to maintain the accuracy with which it approximates the flow. In Figure 4.6 one can also appreciate the deformation of the initial **m**-orthogonal surfaces as they stretch and wrap around the vortex patches. In Figure 4.4 the scattered dipoles do not form discernible surfaces.

We computed the order of accuracy of the impulse method by approximating the same vortex sheets with twice as many impulse vectors as the previous discretization. The final time was chosen arbitrarily as representative of times when the original impulse method is known to yield wrong answers. At other final times, the results were similar. Figure 4.7 shows that the errors in the vortex locations decreased by about a factor of 4. This is an indication of second-order accuracy as one would expect from the midpoint-rule approximation of the vortex flow. In spite of the explicit dependence of the energy $1/2 \sum \mathbf{m}^j \cdot \mathbf{u}(\mathbf{x}^j)$ on the discretization, energy was conserved to within 1.5% of its original value in this computation. The refinement procedure allows the impulse to maintain the initial accuracy in its approximation of the vortex flow, but it is clearly not a practical implementation of the impulse method since the number of particles continually increases without bound. In Figure 4.6 (at time 4.72) there are four times as many particles as there were at $t = 0$.

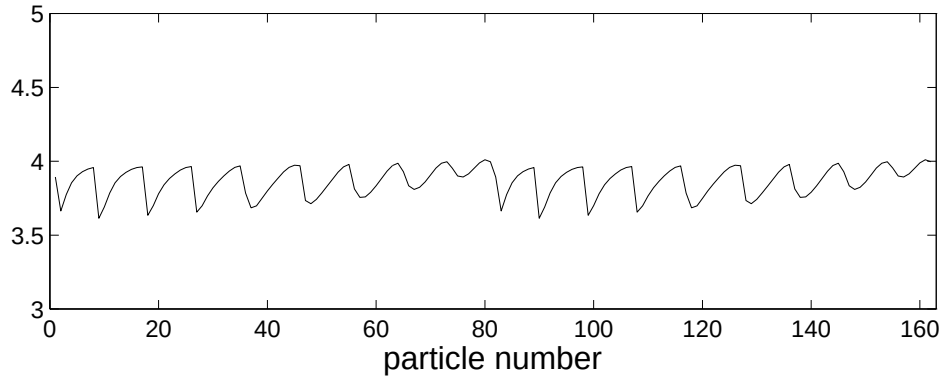

FIG. 4.7. *Comparison of vortex positions at* $t = 4.72$. *The figure shows the ratio of the distances between corresponding vortices given by the impulse method with refinement and the vortex method for* $h = 0.05$ *and* $h = 0.025$.

5. Conclusions. The connection between the velocity field due to vortex blobs and the velocity field induced by impulse blobs has been established. The connection is that the velocity field induced by impulse is a quadrature approximation of the velocity induced by a vortex sheet in two dimensions. An extension of these arguments to three dimensions shows that a large closed loop of vorticity induces a velocity field that can be approximated by an integral over any surface that spans the loop (see [12, 15, 20]). When the integration path (the vortex sheet) is carried by the flow and stretches, the approximation of the line integral loses accuracy as the points along the path become sparse. The severity of the accuracy loss is increased by the singularity of the impulse method kernel. The stretching of the path results in the growth of the magnitude of impulse vectors. This is a manifestation of the growth of the gradient in (2.1) and the effect of the particle redistribution on the accuracy of the gradient difference operators in a Lagrangian setting. It is clear that impulse methods can be less efficient than vortex methods when portions of the vortex sheets have zero vorticity, as in the examples presented here. The impulse method with dynamic refinement was used to illustrate the results and allow long-time implementations of the method. However, it does not seem to be practical for use in interior flows. A variant of the method presented in [15] exploits the nonuniqueness of impulse to maintain the initial accuracy but is not easily extended to three dimensions.

The interpretation of impulse vectors as vortex dipoles with prescribed dipole moment has been explained. The main consequences of this interpretation are that the high-order cutoff functions of vortex methods are the correct cutoff functions for impulse methods and that the role of the cutoffs in the accuracy analysis of vortex methods can be imported into impulse methods. The convergence of the particle locations given by the impulse method to the locations given by the corresponding vortex method (the one that uses the same cutoff parameters) has been demonstrated numerically.

Problems that call for the use of vortex dipoles or ones in which vortex sheets do not suffer extensive stretching are clear candidates for the application of impulse methods. Vortex dipoles have been used to model free-surface motion [3, 4, 2, 19] and to introduce surface forces effects [29, 10]. Impulse variables provide important advantages in this type of application because the equations of motion for impulse

correctly update the dipole strengths. Since forces are rates of change of impulse, the impulse evolution equations can easily be written to include forces. This was done in [16], where the motion of an elastic membrane immersed in an incompressible fluid was tracked. There, the surface forces were due to variable tension, as is the case in applications such as the blood flow in the heart cavities and other problems in physiology [24, 26, 27]. Such applications also require the inclusion of viscous effects. Numerical methods that develop evolution equations for the vortex sheet strength based on Bernoulli's equations are limited to Euler flows. Viscous effects can be included in impulse methods without difficulty [11].

The vorticity induced by the impulse approximation in (3.3) has the property of being solenoidal in any space dimension, which makes it attractive to use an impulse formulation for the creation of vorticity near solid boundaries [34]. However, as the new elements diffuse into the flow interior, they must be converted into vortex elements in order to avoid carrying the computation while extensive stretching of the vortex sheets occurs.

Acknowledgment. I thank A. Chorin for his support while developing this paper.

REFERENCES

[1] C. Anderson and C. Greengard, *On vortex methods*, SIAM J. Numer. Anal., 22 (1985), pp. 413–440.
[2] G. R. Baker, *A test of the method of Fink & Soh for following vortex-sheet motion*, J. Fluid Mech., 100 (1980), pp. 209–220.
[3] G. R. Baker, D. I. Meiron, and S. A. Orszag, *Generalized vortex methods for free-surface flow problems*, J. Fluid Mech., 123 (1982), pp. 477–501.
[4] G. R. Baker, D. I. Meiron, and S. A. Orszag, *Generalized vortex methods for free surface flow problems* II: *Radiating waves*, J. Sci. Comput., 4 (1989), pp. 237–259.
[5] G. K. Batchelor, *An Introduction to Fluid Dynamics*, Cambridge University Press, New York, 1967.
[6] J. T. Beale and A. J. Majda, *High order accurate vortex methods with explicit velocity kernels*, J. Comput. Phys., 58 (1985), pp. 188–288.
[7] T. F. Buttke, *The Hamiltonian structure of 3D fluid flow*, in Proceedings of International Workshop on Vortex Flows and Related Numerical Methods, Grenoble, France, June 15–20, 1992.
[8] T. F. Buttke, *Velicity methods: Lagrangian numerical methods which preserve the Hamiltonian structure of incompressible fluid flow*, in Vortex Flows and Related Numerical Methods, J. T. Beale, G.-H. Cottet, and S. Huberson, eds., Kluwer Academic Publishers, 1993, NATO ASI Series C, Vol. 395, pp. 39–57.
[9] T. F. Buttke and A. J. Chorin, *Turbulence calculations in magnetization variables*, Appl. Numer. Math., 12 (1993), pp. 47–54.
[10] Y. C. Chang, T. Y. Hou, B. Merriman, and S. Osher, *A level set formulation of Eulerian interface capturing methods for incompressible fluid flow*, J. Comput. Phys., 124 (1996), pp. 449–464.
[11] A. J. Chorin, *Numerical study of slightly viscous flow*, J. Fluid Mech., 57 (1973), pp. 785–796.
[12] A. J. Chorin, *Vortex Methods*, Technical Report PAM-593, Center for Pure and Applied Mathematics, University of California, Berkeley, 1993.
[13] A. J. Chorin, *Vorticity and Turbulence*, Springer-Verlag, New York, 1994.
[14] A. J. Chorin and J. E. Marsden, *A Mathematical Introduction to Fluid Mechanics*, Springer-Verlag, New York, 1979.
[15] R. Cortez, *Impulse-Based Particle Methods for Fluid Flow*, Ph.D. thesis, University of California, Berkeley, 1995.
[16] R. Cortez, *An impulse-based approximation of fluid motion due to boundary forces*, J. Comput. Phys., 123 (1996), pp. 341–353.
[17] O. H. Hald, *Convergence of vortex methods* II, SIAM J. Sci. Comput., 16 (1979), pp. 726–755.

[18] O. H. Hald, *Convergence of vortex methods for Euler's equations* III, SIAM J. Numer. Anal., 24 (1987), pp. 538–582.
[19] J. J. L. Higdon and C. Pozrikidis, *The self-induced motion of vortex sheets*, J. Fluid Mech., 150 (1985), pp. 203–231.
[20] J. D. Jackson, *Classical Electrodynamics*, John Wiley & Sons, New York, 1975.
[21] R. Krasny, *Computation of vortex sheet roll-up*, in Vortex Methods, C. Anderson and C. Greengard, eds., Springer-Verlag, Berlin, New York, 1987.
[22] P. Luchini, *Magnetization vector analogy as a reformulation of the equations of fluid mechanics*, AIAA J., 29 (1991), pp. 474–477.
[23] J. H. Maddocks and R. L. Pego, *An unconstrained Hamiltonian formulation for incompressible fluid flow*, Comm. Math. Phys., 170 (1995), pp. 207–217.
[24] M. F. McCracken and C. S. Peskin, *A vortex method for blood flow through heart valves*, J. Comput. Phys., 35 (1980), pp. 183–205.
[25] V. I. Oseledets, *On a new way of writing the Navier-Stokes equation: The Hamiltonian formalism*, Commun. Moscow Math. Society, 44 (1989), pp. 210–211.
[26] C. S. Peskin, *Mathematical Aspects of Heart Physiology*, Lecture Notes, Courant Institute of Mathematical Sciences, New York, 1975.
[27] C. S. Peskin, *Numerical analysis of blood flow in the heart*, J. Comput. Phys., 25 (1977), pp. 220–252.
[28] E. G. Puckett, *A review of vortex methods*, in Incompressible Computational Fluid Mechanics, R. Nicolaides and M. Ginzburger, eds., Cambridge University Press, London, 1992.
[29] D. I. Pullin, *Numerical studies of surface tension effects in nonlinear Kelvin-Helmholtz and Rayleigh-Taylor instability*, J. Fluid Mech., 119 (1982), pp. 507–532.
[30] P. H. Roberts, *A Hamiltonian theory for weakly interacting vortices*, Mathematica, 19 (1972), pp. 169–179.
[31] P. H. Rouhi, *Poisson Brackets for Point Dipole Dynamics in* 3*D Euler Flow*, 1990, manuscript.
[32] P. G. Saffman, *Vortex Dynamics*, Cambridge University Press, London, 1992.
[33] J. A. Sethian, *A brief overview of vortex methods*, in Vortex Methods and Vortex Motion, K. E. Gustafson and J. A. Sethian, eds., SIAM, Philadelphia, 1991.
[34] D. Summers and A. J. Chorin, *Numerical vorticity creation based on impulse conservation*, Proc. Nat. Acad. Sci. U.S.A., 93 (1996), pp. 1881–1885.